Stratosphere-troposphere evolution during polar vortex intensification

Varavut Limpasuvan,[1] Dennis L. Hartmann,[2] David W. J. Thompson,[3] Kumar Jeev,[4] and Yuk L. Yung[5]

Received 31 May 2005; revised 14 September 2005; accepted 29 September 2005; published 17 December 2005.

[1] Stratosphere-troposphere evolution associated with polar vortex intensification (VI) events is examined during the Northern Hemisphere winter. The incipient stage of a VI event is marked by anomalously low wave activity and descending westerly anomalies over the depth of the polar stratosphere. Reduced poleward planetary wave heat flux occurs as the circumpolar wind becomes strongest and pressure anomalies penetrate toward the surface. Descending pressure patterns project strongly onto the positive state of the Northern Hemisphere Annular Mode (NAM). Concurrently, anomalous poleward momentum flux develops in the upper troposphere, and the related tropospheric mean meridional circulation maintains the attendant wind and temperature anomalies against surface drag. The gross behavior of the composite VI event is similar in shape but opposite in sign to that associated with sudden stratospheric warming events (SSWs). However, the descent of the wind and temperature anomalies over the VI life cycle is generally weaker and slower than its SSW counterpart preceding the maximum vortex anomaly. Similarly, after the maximum wind event, the weakening of the winds is faster than the strengthening of the winds after a SSW. This is because stratospheric wind reduction anomalies are produced by wave driving, which can be rapid, and increases in wind speed are associated with the radiative cooling of the polar cap, which happens more gradually. While the contributions of the anomalous momentum fluxes by the quasi-stationary and synoptic eddies are similar to SSWs, the much stronger anomalous momentum flux observed during VI can be attributed to the larger role of eddies with timescales between 15 and 40 days and of wave number 2 scale. Notable differences between VI and SSW appear in the tropical region. In particular, anomalous vortex intensification seems to occur preferentially during La Niña conditions.

Citation: Limpasuvan, V., D. L. Hartmann, D. W. J. Thompson, K. Jeev, and Y. L. Yung (2005), Stratosphere-troposphere evolution during polar vortex intensification, *J. Geophys. Res.*, *110*, D24101, doi:10.1029/2005JD006302.

1. Introduction

[2] The stratosphere has been historically viewed as a relatively passive component of the climate system. However, over the past several years, mounting evidence suggests that stratospheric variability does, in fact, play an important role in driving climate variability at Earth's surface [e.g., *Quiroz*, 1977; *Hartley et al.*, 1998; *Kuroda and Kodera*, 1999; *Hartmann et al.*, 2000; *Baldwin and Dunkerton*, 2001; *Black*, 2002]. In the Northern Hemisphere (NH), the linkage between the stratosphere and troposphere appears most obvious when the stratospheric polar vortex undergoes unusually strong variation in wind strength and temperature.

[3] Conditions of anomalously weak stratospheric polar vortex are associated with "sudden stratospheric warming events" (SSWs) in which the polar stratospheric temperature rises dramatically over a short time period [e.g., *McIntyre*, 1982; *Andrews et al.*, 1987]. *Quiroz* [1977], *O'Neill and Taylor* [1979], and *O'Neill* [1980] first presented evidence for the appearance of near-surface temperature anomalies in conjunction with the major NH SSW event of 1976–1977. Recently, *Limpasuvan et al.* [2004, hereinafter referred to as LTH] noted that the composite SSW life cycle is preceded by preconditioning of the upper stratospheric circulation and by anomalous planetary-scale wave forcing at stratospheric and near-surface levels. As the SSW matures (and the vortex becomes weakest), the largest stratospheric zonal flow and temperature anomalies and the region of largest wave driving descend throughout the depth of the stratosphere, as a result of wave mean flow interactions. When the anomalous wave driving reaches the lowermost stratosphere, the associated flow anomalies appear to penetrate the tropopause, eliciting substantial

[1]Department of Chemistry and Physics, Coastal Carolina University, Conway, South Carolina, USA.
[2]Department of Atmospheric Sciences, University of Washington, Seattle, Washington, USA.
[3]Department of Atmospheric Science, Colorado State University, Fort Collins, Colorado, USA.
[4]Department of Earth and Planetary Sciences, Johns Hopkins University, Baltimore, Maryland, USA.
[5]Division of Geological and Planetary Sciences, California Institute of Technology, Pasadena, California, USA.

0148-0227/05/2005JD006302$09.00

anomalous responses in both wave propagation and the mean meridional circulation at tropospheric levels [*Haynes et al.*, 1991; *Kuroda and Kodera*, 1999; *Shindell et al.*, 1999]. In contrast to the waves that initiate the stratospheric warming, the anomalous tropospheric wave forcing during the mature phase of the SSW is associated primarily with waves smaller than planetary-scale.

[4] The key to downward stratospheric influence (and its amplification) lies in the projection of the descending flow anomalies onto the tropospheric component of the Northern Hemisphere Annular Mode (NAM) [*Baldwin and Dunkerton*, 1999, 2001]. The NAM is the dominant pattern of internal tropospheric variability and is characterized by out-of-phase fluctuations in the strength of the zonal mean wind between centers of action located near 35 and 55 degrees latitude [e.g., *Thompson and Wallace*, 1998].

[5] As shown by *Baldwin and Dunkerton* [2001], downward stratospheric influence on the troposphere also appears to be significant when the polar vortex undergoes unusual intensification with significant polar cooling. Unlike the anomalous vortex weakening case (i.e., SSW), the surface patterns take on the (positive) NAM signature as the vortex strength becomes most intense. *Ambaum and Hoskins* [2002] argued that significant positive Arctic potential vorticity anomaly related to vortex strenghtening can significantly raise the polar tropopause by geostrophic and hydrostatic adjustment. Through vortex stretching, the raised tropopause can then lead to significant Arctic low-pressure anomaly on the troposphere that projects onto the positive NAM. Model results of *Polvani and Kushner* [2002] similarly suggested that strong cooling of the polar winter stratosphere is linked to the poleward shift and strengthening of the tropospheric jet and the accompanied NAM-like surface pressure pattern.

[6] In the present study, we extend the observational work of *Baldwin and Dunkerton* [2001] and LTH by examining, in detail, the atmospheric evolution and wave fluxes during stratospheric vortex intensification events (VIs, hereinafter). This is the first comprehensive examination of vortex intensification events. We focus on the mean circulation and wave forcing in the troposphere and stratosphere and their implications for the surface NAM. By showing the various dynamical quantities during the vortex intensification process, our study complements the work of LTH that focused on the vortex breakdown during SSWs. We show that, as is the case with sudden stratospheric warmings, VI events are associated with enhanced anomalous momentum fluxes by planetary-scale quasi-stationary and transient waves in the upper troposphere, and that these anomalous wave fluxes are important in establishing and maintaining the tropospheric wind anomalies related to NAM. We also show that in contrast to SSW, VI events have a relatively long onset timescale. We observe that anomalous vortex intensification tends to occur more frequently during La Niña events. We also note that most El Niño winters tend to be associated with SSW events.

2. Data and Analysis

[7] The study uses 44 years of reanalysis data (1958–2001) from the National Center for the Environmental Prediction/National Center for Atmospheric Research (NCEP/NCAR) [*Kalnay et al.*, 1996] and the European Centre for Medium-Range Weather Forecasts (ECMWF ERA-40). All anomalies presented in this study are computed as departures from the daily climatological annual cycle determined from the entire record. Variability in the strength of the stratospheric polar vortex is defined on the basis of the leading Principal Component (PC) time series of daily zonal mean zonal wind anomalies at 50 hPa during the extended wintertime (October–April). The resulting PC time series explains about 54% of the total variance in the 50-hPa zonal mean zonal wind field, and is hereinafter referred to as the Stratospheric Zonal Index (SZI), the same as in LTH. The corresponding first Empirical Orthogonal Function (EOF) mode is well separated from the higher modes on the basis of the criterion of *North et al.* [1982]. Such mode separation is not observed for PC time series (and EOFs) at higher levels (e.g., 10 hPa). For consistency with LTH, the SZI is computed using the NCEP/NCAR reanalyses.

[8] The anomalous intensification of the polar vortex is determined by the amplitude of the 15-day low-pass SZI. Considerable strengthening of the vortex commences when the low-pass SZI surpasses one standard deviation above its long-term mean. The central date of a VI event (referred to as day 0) is the midpoint between the day when the SZI rises above +1 standard deviation and when it returns again below +1 standard deviation (at least 5 days away). The central date corresponds closely to the time when the polar westerly strength and cooling are greatest (see Figure 1b, left plots). Each intensification event is taken to be 81 days in duration (40 days before and after day 0) in parallel to SSWs of LTH.

[9] Overall, 41 events were chosen on the basis of the above criteria. The central dates associated with these events occur between early December and early April (Figure 1a). A representative life cycle of the intensification process is defined as the composite average of these 41 events. In this paper, we present the life cycle by dividing it into five 15-day average increments that reflect the onset (days −37 to −23), growth (days −22 to −8), maturation (days −7 to +7), decline (days +8 to +22), and decay (days +24 to +37) of a typical VI. Here, the negative (positive) times indicate days prior to (after) the central date (or day 0). We also present the life cycle as altitude-time sections of (cosine-weighted) latitudinally averaged variables for the entire 81-day period. Unless noted in the figure captions, gray shading indicates areas with 95% confidence level (based on the *t*-statistic).

[10] As shown in Figure 1b (left plots), the composite VI life cycle of the ECMWF *total* zonal mean temperature at 85°N and zonal mean zonal wind at 70°N exhibit a gradual buildup in vortex strength and cooling toward day 0 and relatively quicker recovery thereafter. The slow initial intensification is expected as the stratosphere undergoes gradual thermal relaxation. This behavior differs markedly from the SSW case in which the total temperature and wind field exhibit rapid warming in the middle stratosphere and vortex weakening on the timescale of a few weeks around day 0 (Figure 1c, left plots). This apparent difference can be attributed to significantly weaker and less rapid increase of polar temperature and wind anomalies of VI (compare Figure 1b (right plots) with Figure 1c (right plots)). The

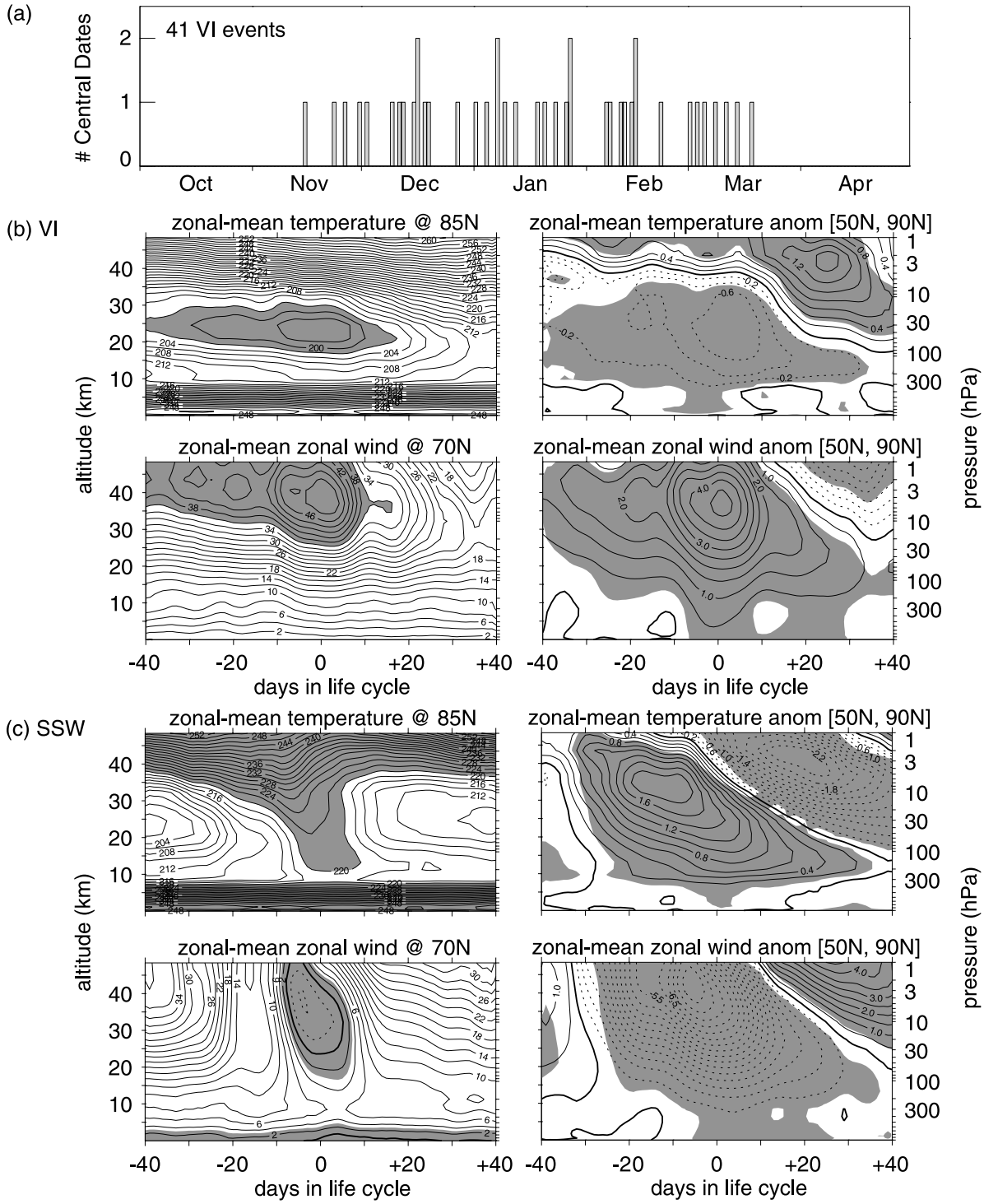

Figure 1. (a) Occurrence of the 41 central dates for vortex intensification. From left to right, the year corresponding to each bar is *1971*, *1988*, *1990*, *1986*, 1964, 1967, 1973, 1999, *1971*, 1975 and 1991, 1992, *1982*, 1972, *1962*, *1984*, 1963 and *1990*, 1983, *1976*, *1965*, 1993, *1986*, *1984*, *1962* and *1990*, 1961, 1974, 1979, 1959, *1965*, *1988* and *1994*, 1996, *1986*, *1976*, 1995, *1965*, *1994*, *1982*, 1960. The italicized years indicate the presence of more than one central date. (b) ECMWF total zonal mean temperature at 85°N (top left plot) and zonal mean zonal wind at 70°N during the composite life cycle of vortex intensification (VI) (bottom left plot). Temperature less than 202 K and wind amplitude greater than 36 m/s are shaded. ECMWF zonal mean temperature anomalies and zonal mean zonal wind anomalies (averaged from 50° to 90°N) during VI (right plots). (c) Same as Figure 1b except for sudden stratospheric warming (SSW). Temperature greater than 220 K and wind amplitude lesser than 3 m/s are shaded. Negative contours are given as dashes. Shading on the right indicates areas with 95% confidence level (based on the t-statistics).

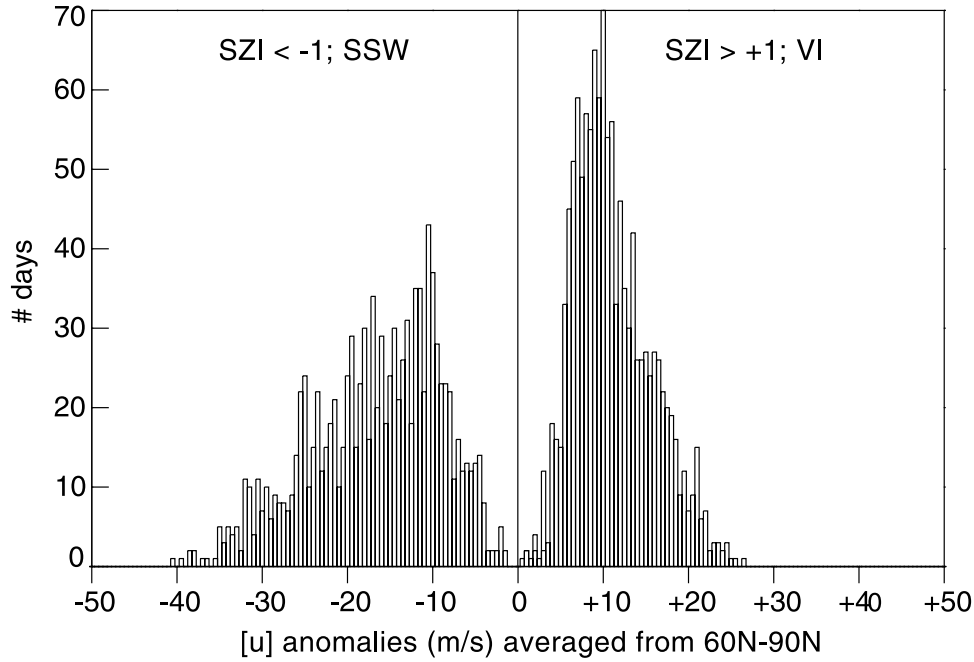

Figure 2. Histogram of the extended wintertime, daily zonal mean zonal wind anomalies at 10 hPa (averaged from 60° to 90°N) during the 41 VI and 39 SSW events. Only wind values corresponding to when SZI > +1 and SZI < −1 are counted.

contrasting nature of SSW and VI is further illustrated in Figure 2 which shows the histogram of the averaged zonal mean zonal wind anomalies when SZI is greater than +1 (corresponding to VI) and lesser than −1 (SSW). The anomalous wind amplitudes are stronger during SSWs but more persistent during VI.

[11] Despite this disparity in onset timing and amplitudes, significant wind and temperature anomalies for SSWs and VIs do extend toward the surface when the anomalies maximize near day 0. As in SSWs, VI anomalies span much of the winter season with a lifetime of about 80 days and downward tilting zero anomaly contour. As such, they are reminiscent of the stratospheric vacillation cycles observed by *Kuroda and Kodera* [1999] and *Kuroda* [2002].

[12] Overall, these characteristics are nearly identical to composite results based on the NCEP/NCAR data below 10 hPa, which is the uppermost limit of the NCEP/NCAR data (not shown). The similarities between results based on these two data sets are observed for all remaining plots shown below. Consequently, for the rest of the paper, we will only present the results from the ECMWF data, which provide additional information about VI and SSW life cycle above 10 hPa.

3. Zonal Mean Evolution

[13] Figure 3 shows the composite evolution of the anomalous zonal mean zonal wind, zonal mean temperature, and the Eliassen-Palm (EP) flux during VI. At onset (top row), weak negative temperature anomalies appear poleward of 70°N and above 10 km along with westerly wind anomalies in the middle-to-upper polar stratosphere, consistent with thermal wind relationship. Weak subtropical easterly wind anomalies accompany the westerly anomalies (forming a dipole pattern) with a node line extending to the surface around 50°N. At this time, anomalous EP-flux divergence in the polar stratosphere corresponds to significant anomalous wind acceleration poleward of 50°N above 100 hPa and weaker-than-normal poleward heat flux (downward wave activity flux anomaly).

[14] During the growth stage and the eventual maturation, the anomalous easterly westerly dipole structure and polar cooling intensify and descend toward the surface. Vortex cooling peaks during the mature stage near 50 hPa and is associated with the strongest polar wind anomalies observed during the life cycle. Similarly, the region of anomalous wind acceleration (EP-flux divergence) becomes more intense during the growth stage and descends down to 30 hPa. The associated stratospheric wave flux is downward implying anomalously low wave activity as the vortex strengthens further via thermal relaxation. Below 100 hPa during the mature stage, anomalous wave fluxes are most intense and directed equatorward (strong anomalous poleward momentum flux) in the upper troposphere between 20° and 70°N.

[15] The cooling and westerly wind anomalies over the polar region weaken considerably during the decline and decay stages. As the core of anomalous polar westerly wind penetrates down toward 50 hPa, the diminishing center of anomalous cooling continues to descend over the pole, reaching 200 hPa during the decay stage. However, despite the prevailing descent, the region of significant wind anomalies that had reached the surface during the mature phase now recedes upward toward the end of the life cycle. The equatorward anomalous wave activity persists with waning amplitudes. During the decline stage, the attendant anomalous wave forcing reveals an anomalous wind accel-

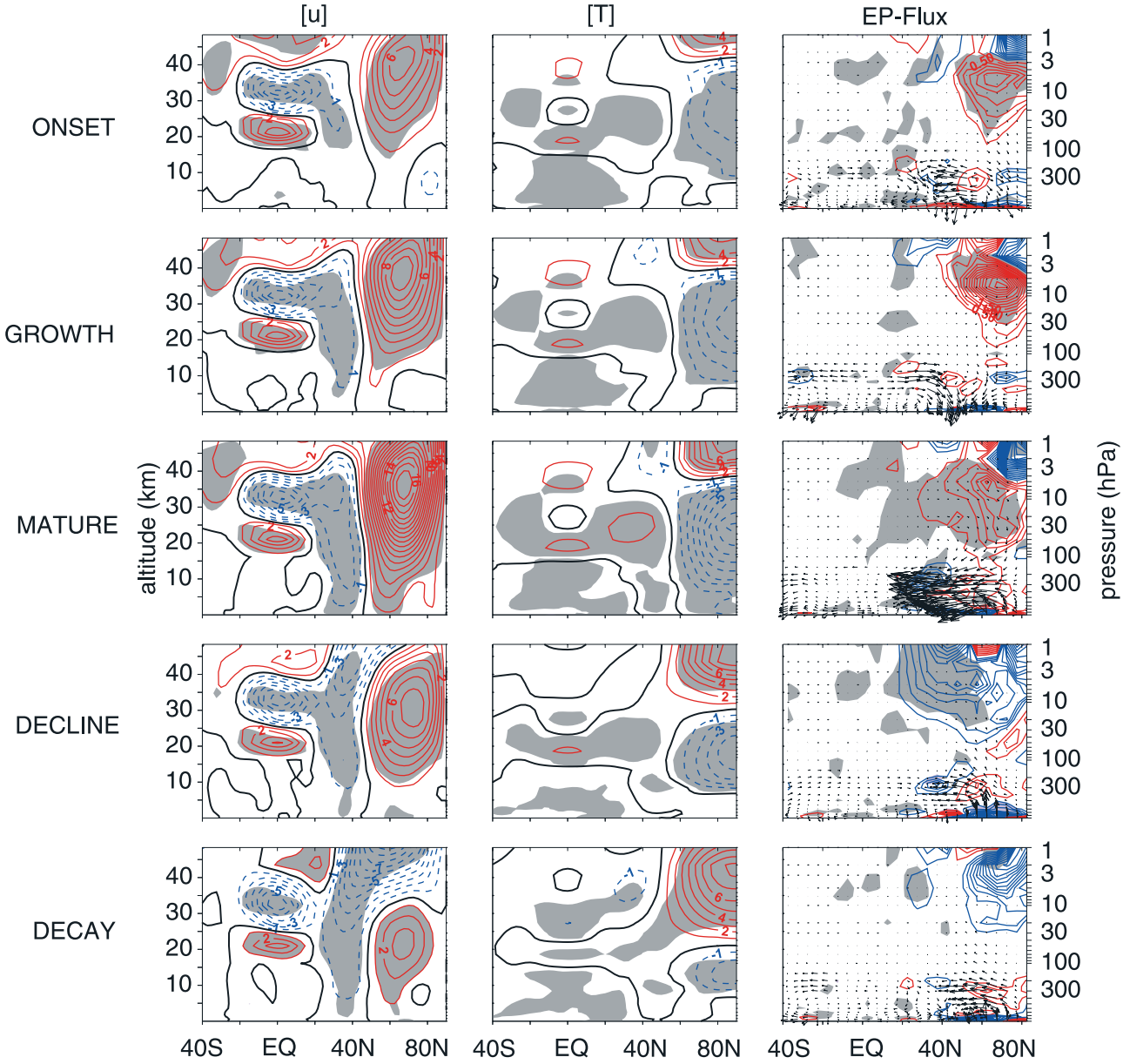

Figure 3. Anomalous (left) zonal mean zonal wind, (middle) zonal mean temperature, and (right) EP-flux with their divergence during VI. Negative contours are given as blue dashes. Zero contours are given as bold solid line. The wind (temperature) contour interval is 1 m/s (1 K). The EP flux divergence (divided by $\rho_o a\cos\theta$, where ρ_o is basic density, a is the Earth's radius, and θ is latitude) is contoured in the right column at every 0.25 m/s/day with deceleration in blue. The vector lengths in the right column are referenced with respect to the top figure in column.

eration-deceleration pair near 300 hPa that is consistent with the westerly easterly dipole structure in the zonal wind.

[16] To first order, these results appear to be the negative of the SSWs life cycle (i.e., a linear response; see Figure 3 in LTH). However, as noted in our discussion of Figures 1 and 2, several key differences are found upon closer examination. The observed westerly easterly dipole pattern in the wind anomalies (with a node near 50°N) appears throughout the 81-day duration. This behavior is consistent with the more gradual buildup and persistence of the wind and temperature anomalies during intensification. In the SSW case, this dipole does not fully appear until very near the time of weakest vortex (i.e., strongest warming during the mature stage). Additionally, the tropospheric temperature anomalies between 10° and 60°N (albeit very weak) are significant and robust during the latter half of the VI life cycle. This behavior is not obvious in the SSW case.

[17] The relatively weak westerly anomalies centered near 50 hPa at the equator, and found throughout the life cycle, are the hallmark of the westerly phase of the equatorial Quasi-Biennial Oscillation (QBO), which favors vortex intensification [*Holton and Tan*, 1980]. On the other hand, the life cycle of sudden stratospheric warmings is marked by the easterly phase of the QBO as shown in LTH.

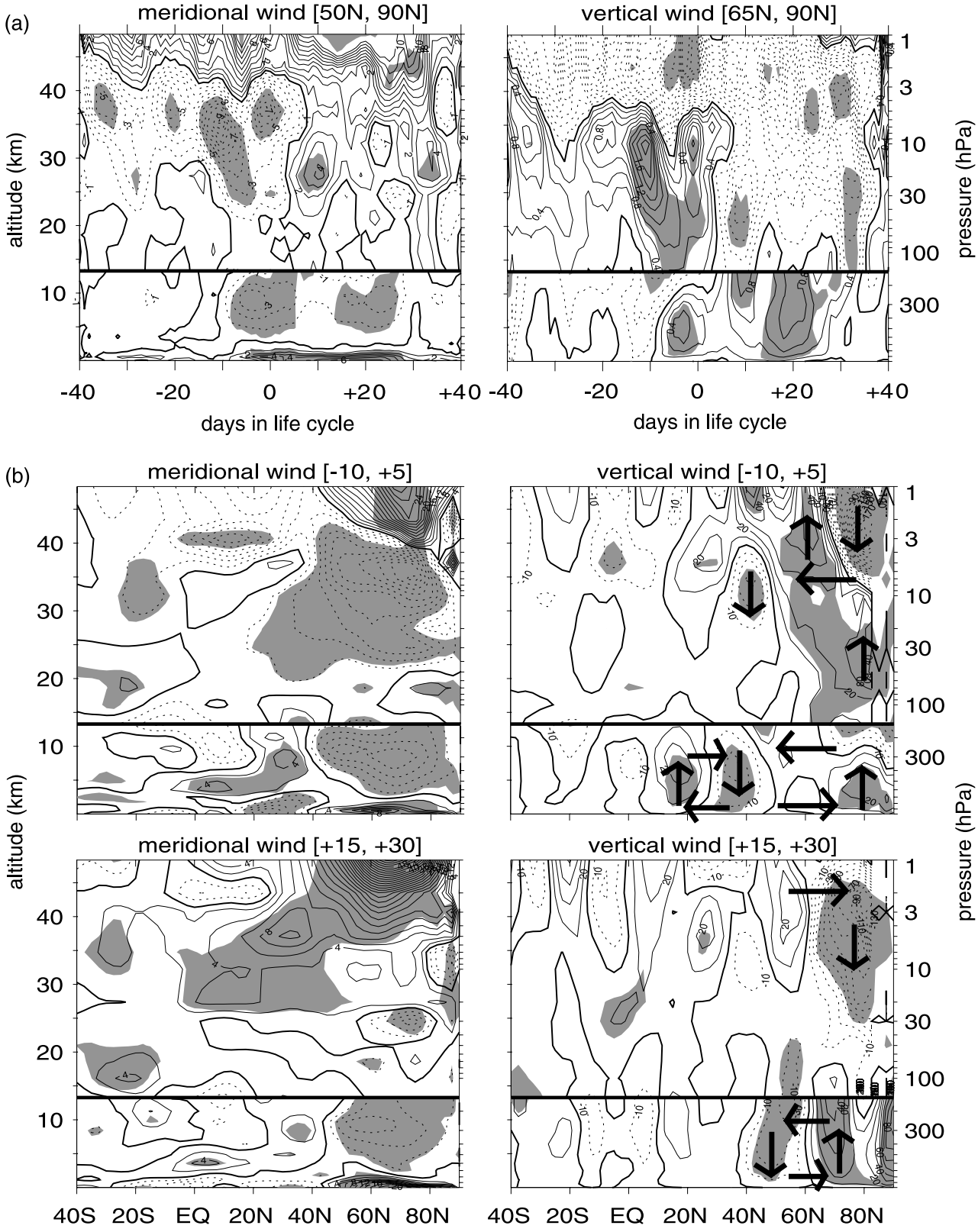

Figure 4. Anomalous zonal mean circulation (below thick horizontal line) and residual zonal mean circulation (above thick horizontal line) during VI. (a) Height-time section of meridional wind (averaged from 50° to 90°N; contoured every 1 cm/s) and vertical wind (averaged from 65° to 90°N; contoured every 2×10^{-2} mm/s). (b) Height-latitude section of meridional and vertical wind averaged over days −10 to +5 (top plots) and over days +15 to +30 (bottom plots) to capture the significant midtropospheric features shown in Figure 4a. The meridional (vertical) wind is contoured every 2 cm/s (10×10^{-2} mm/s). Vertical (horizontal) bold arrows indicate upward/downward (north/south) motion.

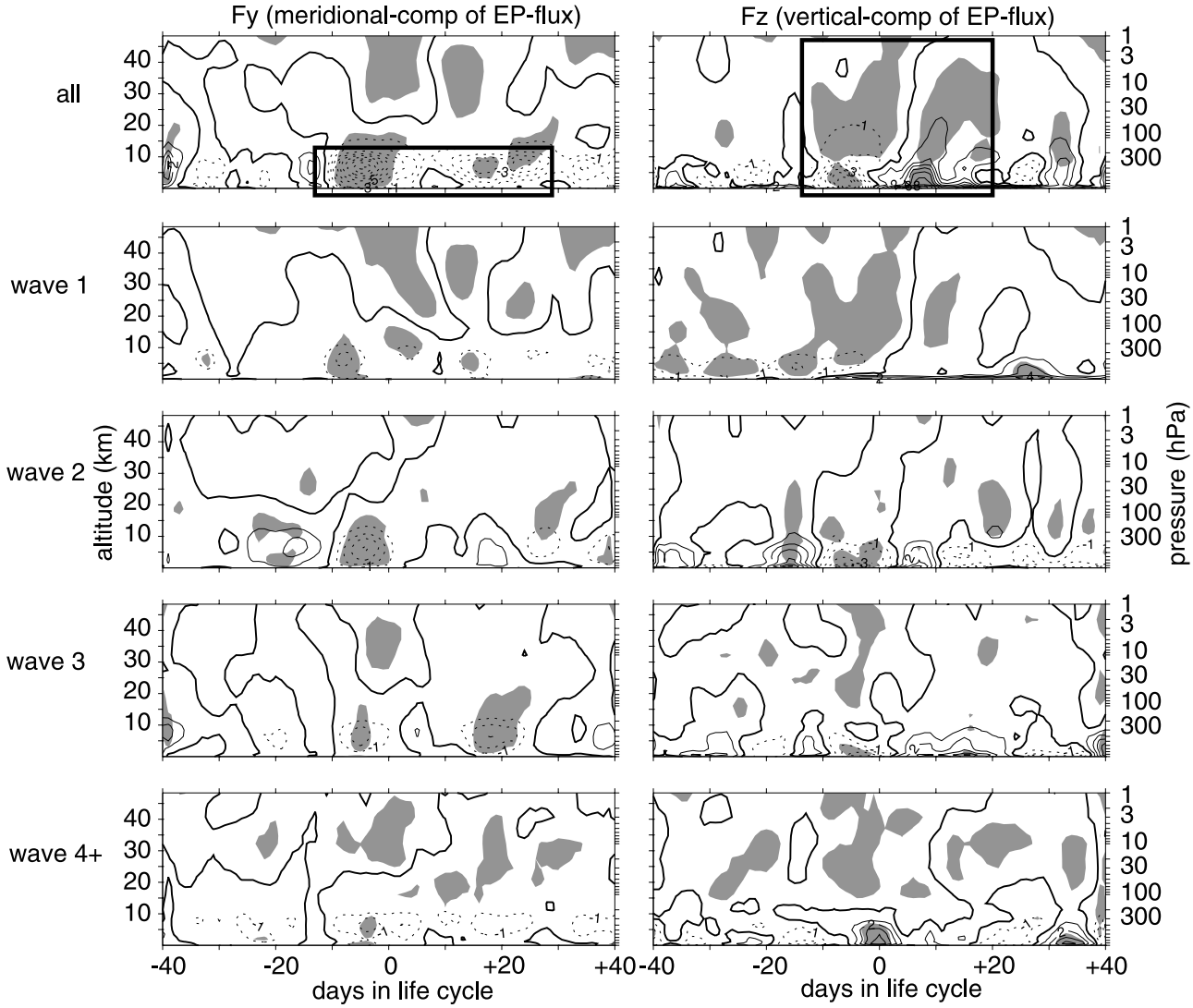

Figure 5. Vertical and horizontal component of anomalous EP-flux (averaged from 50° to 90°N) for all and various wave numbers during VI. Contribution from combined wave numbers greater than or equal to 4 is denoted by "wave 4+." Contours of the vertical component and horizontal component are given every 1×10^4 kg s^{-2} and 1×10^6 kg s^{-2}, respectively. Negative contours are given as dashes. Zero contours are given as bold solid line.

We note that the equatorial wind shear associated with respective QBO phase is much stronger in the current results. We note also that the solar cycle may be as important as the QBO in affecting the vortex variability [e.g., *Naito and Hirota*, 1997; *Ruzmaikin et al.*, 2005]. However, the solar cycle phase was not considered in our analysis.

4. Mean Meridional Circulation

[18] As the VI event approaches its mature stage, the observed anomalous residual mean meridional circulation in the middle stratosphere is upward over the polar region and equatorward in high latitudes. A similar thermally indirect circulation anomaly appears in the tropospheric Eulerian mean circulation. This stratospheric circulation then reverses direction during the decline stage of VI (Figure 4). Overall, the coupling of the lowermost stratospheric circulation anomalies with the troposphere is remarkably linear with respect to SSWs.

[19] The rising motion of the polar stratospheric region is consistent with cooling seen in Figure 3. Such overturning motion develops in response to strong anomalous divergence of EP-flux (associated with unusually low wave activity) in the middle-to-upper stratosphere observed around the same time. The stratospheric circulation reversal shortly after day 0 (Figures 4a and 4b) appears in conjunction with an enhancement in upward stratospheric wave activity, EP-flux divergence, and vortex recovery. The associated (Eulerian mean) tropospheric circulation consists of a counter-clockwise gyre (with respect to the reader) at middle-to-high latitudes, with rising motion over the pole and descent around 40°N. Near the mature stage (days −10 to +5), this tropospheric gyre is accompanied on the equatorward side by a smaller clockwise circulation.

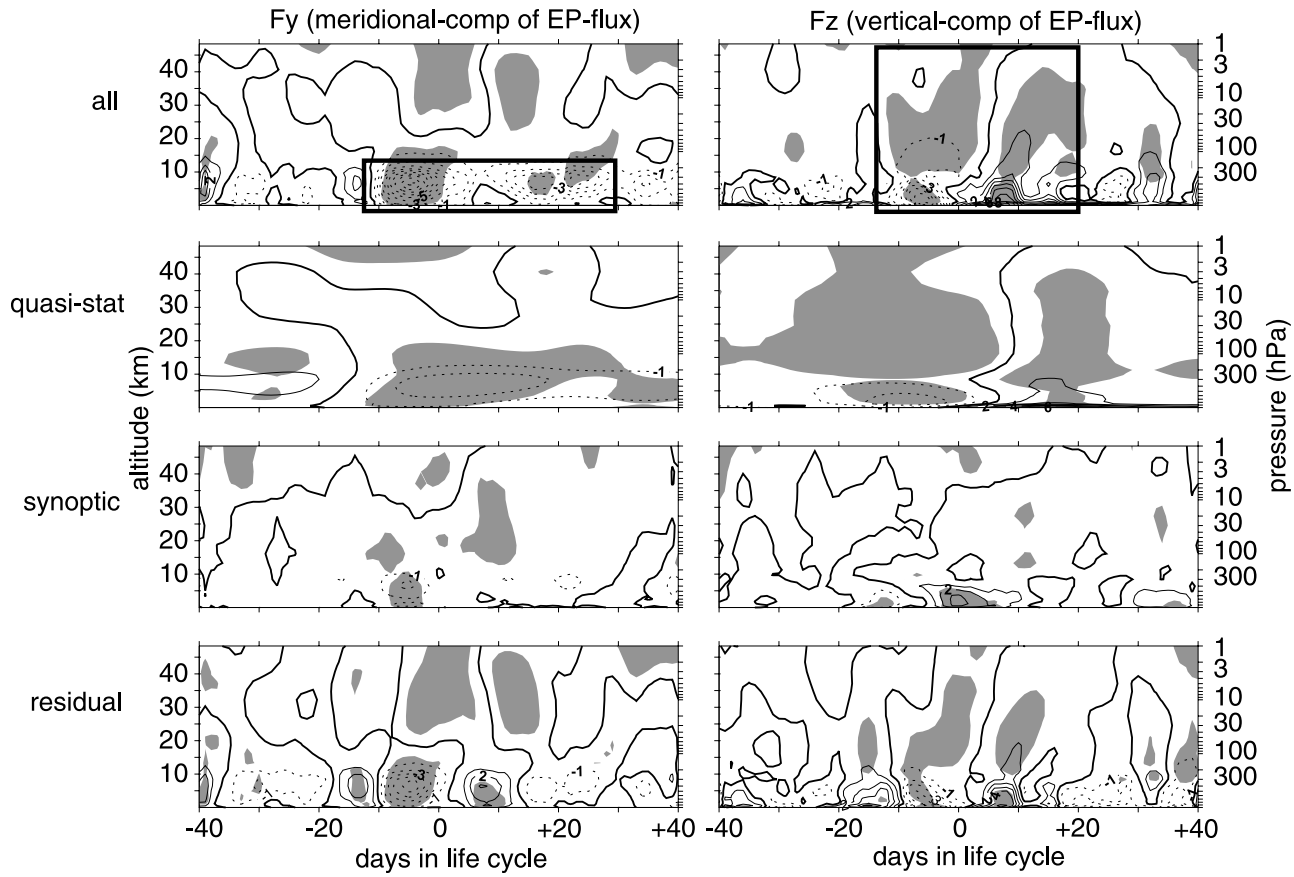

Figure 6. Vertical and horizontal component of anomalous EP-flux (averaged from 50° to 90°N) for all and various time-filtered eddies during VI. The quasi-stationary, synoptic, and residual eddy momentum and heat fluxes (used to calculate the EP-flux) are based on the methodology of *Lorenz and Hartmann* [2003]. The sum of "quasi-stat," "synoptic," and "residual" produces the result for "all" which is identical to that shown in Figure 5. Contour intervals, style, and shading are same as in Figure 5.

[20] The appearance of the tropospheric circulation cell coincides with the pronounced upper tropospheric meridional EP-fluxes (see Figure 3 (right), mature stage). Near 300 hPa, the two significant extrema in the mean meridional wind (see Figure 4a) parallel the anomalous momentum fluxes shown in Figure 5 (top row). Since the Coriolis force acting on the upper tropospheric equatorward (poleward) flow opposes the westerly (easterly) anomalies there, it follows that the tropospheric overturning cell must be driven by the anomalous divergence of the eddy momentum flux (meridional component of the EP-flux vectors). The Coriolis torque acting on the equatorward (poleward) surface wind anomalies helps maintain the lower-tropospheric easterly (westerly) anomalies against frictional dissipation. Thus, while the largest wind anomalies in Figure 3 are found at the stratospheric levels, substantial anomalies are also observed at near surface levels as the result of this overturning tropospheric circulation fostered by strong momentum fluxes.

[21] We note that the circulation related to the easterly shear zone of the QBO is not obvious in the observed stratospheric circulation. With the equatorial cold anomalies between the anomalous easterly westerly dipole pattern observed in Figure 3, QBO theory suggests ascending motion over the center of equatorial cold anomalies, poleward motion around 35 km in the subtropics, and a descending motion around 40°N near 30 km [e.g., *Plumb and Bell*, 1982]. In Figure 4b, we only see a hint of this significant descending motion around 40°N. In the reanalyses data used here, small-scale waves that drive the QBO (like gravity waves) are not explicitly resolved. Their momentum forcings are therefore not well represented in the data, leading to unrealistic equatorial circulation in the stratosphere.

5. Contributions to Wave Fluxes

[22] The temporal evolution of the vertical (Fz) and meridional (Fy) components of the anomalous EP-flux (averaged from 50° to 90°N) are illustrated in Figure 5. The vertical component is proportional to poleward eddy heat flux; the meridional component is proportional to the negative of poleward eddy momentum flux [*Andrews et al.*, 1987]. Consistent with the EP-flux vectors shown in Figure 3, the anomalous momentum fluxes by all waves are poleward (negative Fy) throughout the troposphere during the mature stage and thereafter (rectangular box in Figure 5 (left)). These momentum fluxes correspond closely to the mean meridional circulation in the troposphere shown in Figure 4. The anomalous heat fluxes (and

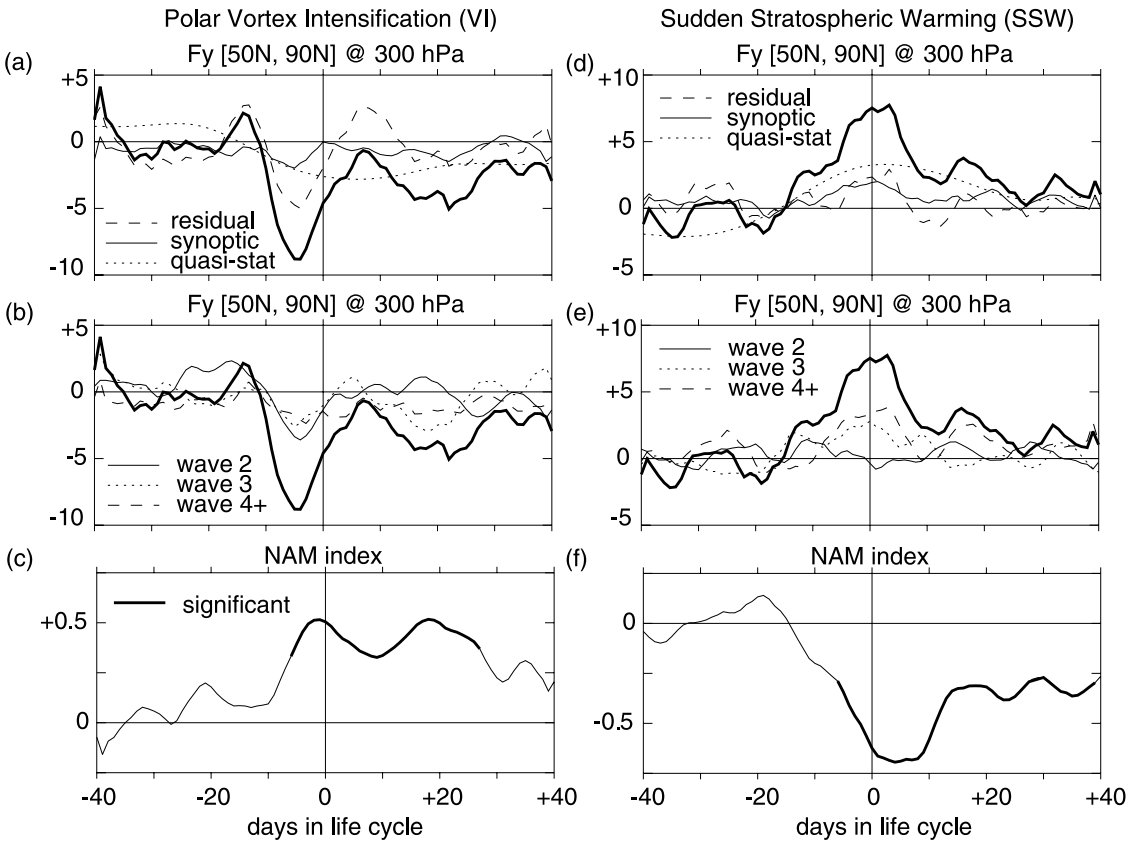

Figure 7. (a–c) Evolution of anomalous momentum flux (averaged from 50° to 90°N) and surface NAM index during VI. (d–f) Same as Figures 7a–7c except for sudden stratospheric warming (SSW).

vertical wave activity) are most pronounced between days −20 and +20 and switch sign in conjunction with the reversal of the anomalous stratospheric circulation shown in Figure 4.

[23] Planetary-scale waves (combined wave numbers 1, 2, 3) make the strongest contribution to the overall anomalous momentum fluxes in the troposphere. Prior to day 0, wave number 2 momentum flux is the most dominant. Wave number 3 contribution becomes pronounced around day +20 as the vortex recovers. The nature of these eddy momentum fluxes is explored further in Figure 6 (left), which shows the temporal decomposition of the eddy fluxes into quasi-stationary timescales (> 40 days), synoptic timescales (<15 days), and residual timescales (defined here as timescales between 15 and 40 days, plus the fluxes associated with interactions with the quasi-stationary and synoptic timescales). As in LTH, the formulation and definition of the time-filtering technique follows directly from *Lorenz and Hartmann* [2003]. Clearly, the dominant planetary-scale eddy momentum fluxes are associated mainly with quasi-stationary and residual timescales.

[24] Prior to day +5, the equatorward heat flux anomaly in the stratosphere is composed largely of reduced wave number 1 flux. After day +5, the wave number 1 activity increases and the associated poleward heat flux weakens the vortex toward climatology (see Figure 3). From Figure 6 (right), the wave number 1 contribution appears to be primarily of quasi-stationary and residual timescales. Below 300 hPa and around the mature stage, the anomalous heat flux is mainly dominated by wave numbers 2 and 3 that are primarily of quasi-stationary and residual timescales. A significant poleward heat flux centered near day 0 is associated with smaller-scale waves (combined wave numbers of 4 and greater) and synoptic timescales (compare "wave 4+" Fz in Figure 5 with "synoptic" Fz in Figure 6). Thus anomalous growth in synoptic wave activity near the surface coincides with the vortex maximum.

[25] The anomalous momentum flux in the upper troposphere is larger in magnitude (∼22%) and peaks slightly earlier in the life cycle than during SSW (see Figure 7). While the contribution of the momentum fluxes by the quasi-stationary and synoptic eddies are similar to SSWs, the much stronger momentum flux can be attributed to the larger role of residual timescale eddies (Figures 7a and 7d). While waves of all spatial scale act in concert in VI (with wave number 2 being largest), the wave number 2 contribution is noticeably absent in SSW, with the largest contribution coming from smaller-scale waves (combined wave numbers 4 and greater; Figures 7b and 7e). Thus, while the eddy momentum fluxes are central to the tropospheric coupling in VIs and SSWs, the decomposition of these momentum fluxes shows noticeable differences.

[26] While the wave number 1 contribution to the anomalous heat flux (albeit of opposite sign) is similar to SSW, the overall behavior shown in Figures 5 and 6 is quite different from that case. As shown in LTH, the significant anomalous heat flux is much stronger throughout the SSW life cycle, with stronger-than-normal upward wave activity

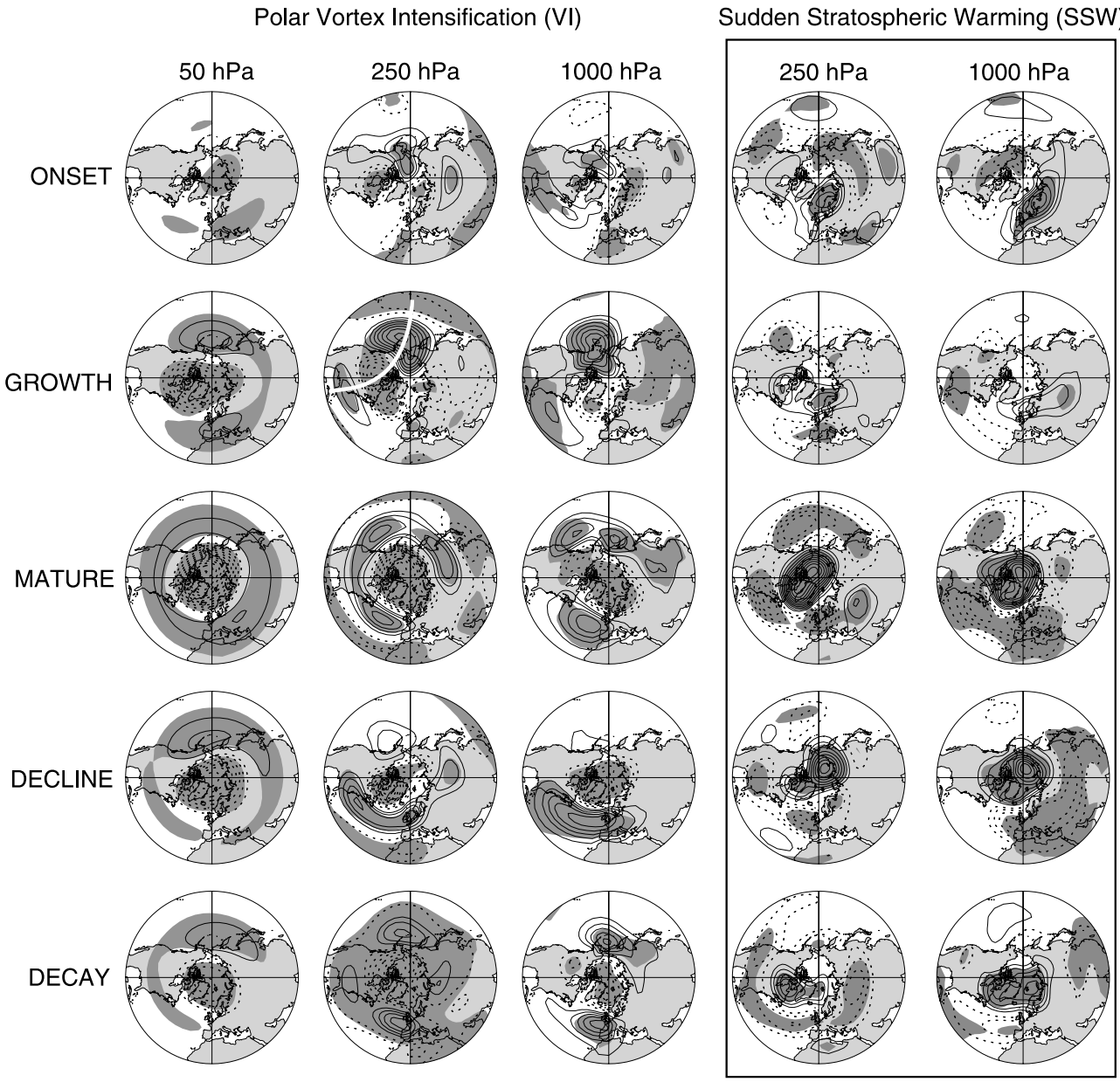

Figure 8. Geopotential height anomalies (in decameters, dam) during VI. The contour interval is 3 dam, 1 dam, and 0.5 dam for 50 hPa, 250 hPa, and 1000 hPa, respectively. Negative anomalies are shown as dashes. The open arc (on growth phase at 250 hPa of VI) draws attention to a pattern analogous to the PNA. Corresponding 250-hPa and 1000-hPa patterns are shown in rectangular box for sudden stratospheric warming.

(poleward heat flux) escalating toward day 0 followed by a period of weaker-than-normal upward wave activity as the vortex recovers. Prior to day 0, the anomalous heat flux (and stratospheric wave forcing) during SSW appears in two distinct episodes: early in the life cycle, the first episode strongly reduces the zonal wind in the upper stratosphere during the preconditioning phase of the warming, while the second burst (around the time of strongest warming) is associated with secondary wind reduction and the penetration of flow anomalies toward the surface. For VI, the vortex simply cools gradually toward day 0 because of lack of wave activity in the stratospheric polar region. Stratospheric wave forcing is noticeably absent before day −20 during VI, and strong anomalous heat (and momentum) flux only appears near day 0 as the wind and temperature anomalies extend toward the surface.

6. Nonzonal View and NAM

[27] The dipole structure in the wind anomalies shown in Figure 3 bears strong resemblance to the wind fluctuation attributable to the positive phase of the NAM [e.g., *Thompson and Wallace*, 1998; *Limpasuvan and Hartmann*, 2000]. The associated jet stream is anomalously northward and the anomalous zonal mean wind structure has a node near 50°N with westerly (easterly) winds on the poleward

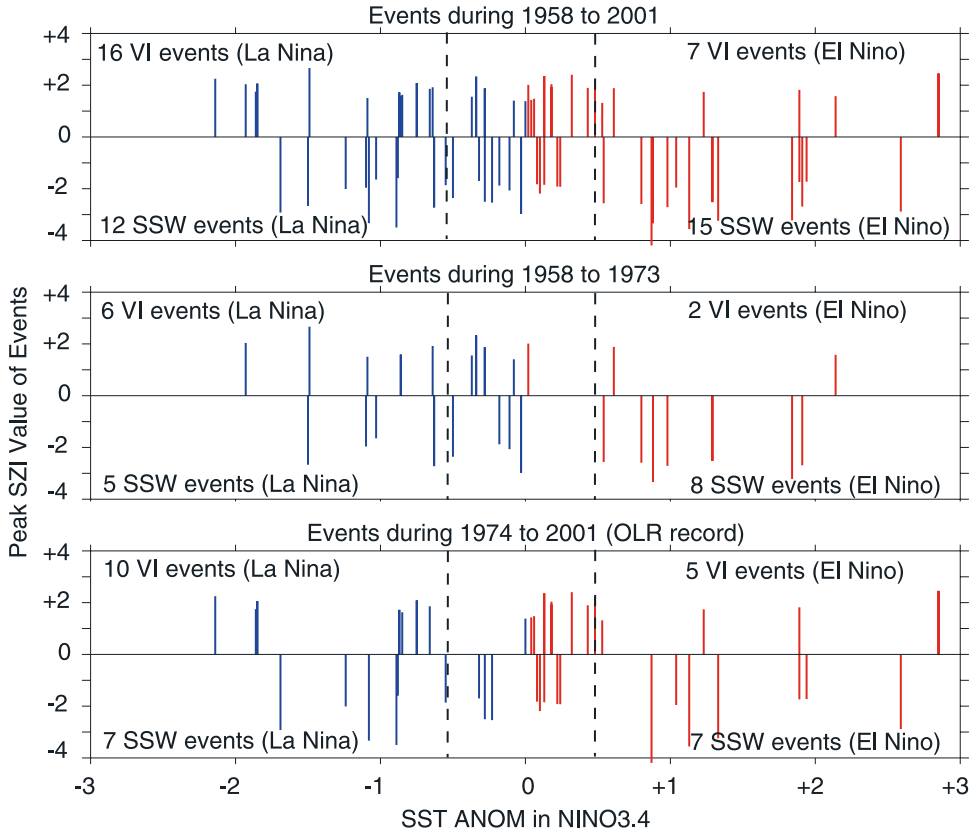

Figure 9. Occurrence of vortex intensification (VI) and stratospheric sudden warming (SSW) versus the NINO3.4 index. El Niño is defined when NINO3.4 > = 0.5. La Niña is defined when NINO3.4 < = −0.5. Size of vertical bars represents the SZI amplitude. Blue (red) bars denote when the NINO3.4 value is negative (positive).

(equatorward) side. As the mature phase approaches and the vortex greatly intensifies, the composite daily surface NAM index (based on the 1000 hPa height) indeed becomes positive and significantly larger than previous stages (Figure 7c). The rapid increase in surface NAM index around day 10 coincides with (1) the extension of the wind anomalies to the surface observed in Figure 3 and (2) the tremendous growth in poleward momentum flux (as summarized in Figure 7a). On the basis of the observed mean meridional circulation in the troposphere, the bias of the surface NAM index is driven and maintained by the Coriolis torques associated with the mean meridional flow near the surface (see Figure 4). Note that the index remains significantly positive until around day +30 consistent with the significant momentum flux around day +20. Such persistence of the surface NAM related to the vortex variation was noted by *Baldwin and Dunkerton* [2001], *Ambaum and Hoskins* [2002], *Norton* [2003], and LTH.

[28] The amplitude rise in the surface NAM index along with the concurrent growth of anomalous momentum flux after day −10 is analogous to the SSW case (Figures 7c and 7f). However, we note that the significant NAM index in the present case is smaller in magnitude but is slightly more persistent. As remarked earlier, we note a stronger contribution by residual timescale eddies in the anomalous momentum flux during VIs than during SSWs.

[29] The connection of VI to NAM can be further demonstrated by the evolution of the zonally varying, anomalous geopotential height field at 1000, 250, and 50 hPa (Figure 8). Clearly, as the mature stage approaches, the height patterns become more barotropic (e.g., similar features at all levels shown) and dominated by a higher degree of zonal symmetry consistent with *Baldwin and Dunkerton* [2001]. This "ring-like" pattern near the surface (during the mature phase) is very similar to the canonical NAM pressure pattern shown by *Thompson and Wallace* [1998] with anomalous low pressure over much of the Arctic and anomalous highs in the surrounding latitudes (with centers near the northern Pacific and Atlantic). This annular structure tends to dominate the height patterns for much of the remainder of the life cycle, although the high anomalous height features show strong variations as indicated by the surface NAM index (Figure 7c).

7. Connections to ENSO

[30] Another difference between SSWs and VIs is observed in the 250 and 1000 hPa height composite. In the western hemisphere, the height field takes on a Pacific North American-like (PNA) pattern during the growth phase (see marked open arc in Figure 7, 250 hPa). This pattern evolves into the NAM during the mature phase and subsequently has larger amplitude in the North Atlantic sector. Such evolution is not present in the SSW height composite (Figure 8). The initial PNA-like appearance suggests that tropical forcing and the El Niño–

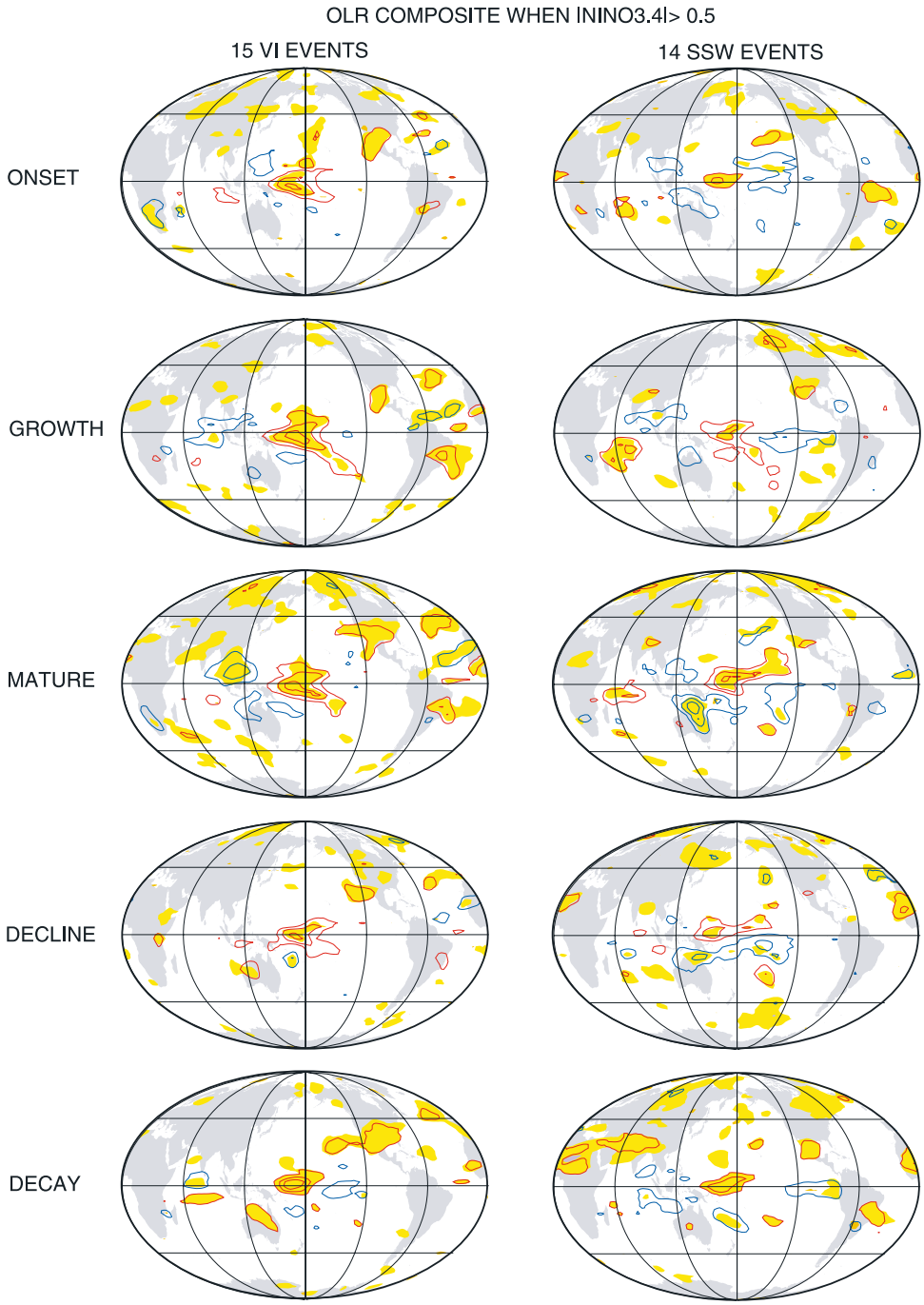

Figure 10. Composite of anomalous outgoing longwave radiation (OLR) during (left) VI and (right) stratospheric sudden warming. Contour interval is 6 W/m^2, with positive (negative) contour in red (blue). Yellow shading indicates areas with 95% confidence level.

Southern Oscillation (ENSO) may play a role in vortex variability.

[31] Figure 9 explores the relationship between the phase of ENSO and anomalous vortex variation, as defined by the SZI. To diagnose the anomalous sea surface temperature anomalies related to ENSO, we use the monthly index of sea surface temperature averaged over 5°N–5°S, 120°–170°W region (the "NINO3.4 index") from the National Ocean and Atmosphere Administration (NOAA) Climate Prediction Center. The months of the largest SZI magnitude

Table 1. Vortex Response to ENSO (October to April)[a]

	SSW	VI	Neither
18 El Niño Winters	12	5	1
22 La Niña Winters	8	10	4

[a]Extended winters identifiable with El Niño and La Niña are partitioned into their vortex responses. Only events unique to a given extended winter are counted.

for the 41 VI events (upward bars) and 39 SSW events (downward bars) are identified with the corresponding NINO3.4 index values. The blue (red) colored bars represent events that occur when the concurrent SST index is negative (positive). The length of the bars indicates the peak SZI value during each event. As there are multiple events in some months of some years, the total number of bars shown is less than 41 (or 39) as the others are plotted over since they occur on the same month. Consistent with Figures 1 and 2, bars representing SSW tend to be longer than VI bars.

[32] El Niño (La Niña) is identified when the NINO3.4 index is greater (lesser) than positive (negative) 0.5 (marked by the vertical dashed lines in Figure 9). For the entire analyzed period (1958–2001), we see that of the 23 VI events that occur during significant ENSO events (beyond ±0.5), nearly 70% of those events correspond to La Niña (Figure 9, top). Overall, the ratio of La Niña to El Niño during VI is about 2:1. This ratio is larger during 1958–1973. On the other hand, the 27 SSWs during mature ENSO are more evenly divided between El Niño and La Niña (with slight bias toward El Niño).

[33] We observe the dominance of La Niña during vortex variation by performing the life cycle composite of the daily NOAA Interpolated Outgoing Longwave Radiation anomalies (OLR [*Liebmann and Smith*, 1996]). The OLR data set has a global spatial coverage with a 2.5° longitudinal and latitudinal resolution. A composite for 15 VI events over the 1974–2001 period (Figure 9, bottom, and Figure 10, left) clearly reveals enhanced convection in the western tropical pacific consistent with La Niña. For the available 14 SSW events during 1974–2001, the dominant ENSO phase is not obvious as there are nearly equal numbers of La Niña and El Niño years in the SSW sample.

[34] In all, 18 (22) extended winters in the data were identified as El Niño (La Niña). As shown in Table 1, during El Niño winters, SSWs occur more than twice as often as VIs. During La Niña winters, VI is slightly more frequent than SSWs. However, consistent with Figure 9, two thirds of VI events occur during La Niña winters. In Table 1, multiple SSW and VI events during an extended winter are counted as one so the numbers of events are less than in Figure 9. Additionally, several winters identifiable with strong ENSO events exhibit neither weak nor strong vortices. As the number of years is small, the statistical uncertainty in the numbers in Table 1 is rather large. If the probability of a SSW in any year is assumed to be 0.5, then the preference of SSW events for El Niño years barely passes a 95% significance test. Such preference is similar to the model study of M. Taguchi and D. L. Hartmann (Change in the occurrence frequency of stratospheric sudden warmings with ENSO-like SST forcing as simulated by WACCM, submitted to *Journal of Climate*, 2005, hereinafter referred to as Taguchi and Hartmann, submitted manuscript, 2005).

8. Summary and Discussion

[35] In light of recent interest in large-scale stratospheric-tropospheric coupling, this study presents the atmospheric flow and the eddy heat and momentum fluxes throughout the stratosphere and troposphere during polar vortex intensification events. Results shown here complement the study of LTH and detail the roles of wave fluxes hinted at in *Baldwin and Dunkerton* [2001]. While noting the gross linear relationship between composite behaviors during SSW and VI episodes, we highlight key similarities and differences in wave and atmospheric flow.

[36] Although no less significant than the SSWs, the growth of polar wind and temperature anomalies during VIs is much weaker and slower, which may explain why they have received less attention. Changes in VI total wind and temperature are much less dramatic than SSW conditions. This slow growth is related to the anomalously low wave activity in stratosphere during the early stages of VI and is indicative of the slow cooling of the vortex via thermal relaxation. Conversely, after the maximum wind event, the weakening of the winds is faster than the strengthening of the winds after SSW. This is because wind reduction anomalies are produced by wave driving, which can be rapid, and increases in wind speed are associated with radiative cooling of the polar cap, which happens more gradually. Regardless, both SSW and VI exhibit descending wind and temperature anomalies that upon reaching the lowermost stratosphere can project onto the surface NAM and elicit dramatic response in both mean meridional circulation and wave propagation [*Kodera et al.*, 1996; *Baldwin and Dunkerton*, 1999, 2001; *Kuroda*, 2002].

[37] As in SSWs, the anomalous momentum flux in the upper troposphere becomes very prominent as the intensification process climaxes and anomalies penetrate across the tropopause. While the contribution of the anomalous momentum fluxes by the quasi-stationary and synoptic eddies are similar to SSWs, the stronger anomalous momentum flux observed during VI can be attributed to the larger role of residual timescale eddies (Figure 7). With respect to SSWs, the wave number 2 contribution to the eddy momentum flux makes a much large contribution during the mature stage of VI. In contrast, the largest contribution to momentum during SSWs comes from smaller-scale waves (combined wave numbers 4 and greater).

[38] Like SSW, upper tropospheric anomalous momentum flux appears in conjunction with the anomalous (Eulerian) mean meridional circulation cells that are organized throughout the troposphere as the VI wind anomalies extend toward the surface. In the upper troposphere, converging meridional flow toward 50°N opposes the anomalous convergence of the eddy momentum flux in middle latitudes. Near the surface, the diverging flow (with northward in the polar region and equatorward in low latitude to midlatitude) helps maintain the wind anomalies against frictional dissipation through the associated Coriolis torque. Anomalous upward motion over the pole and downwelling in the midlatitudes complete the overturning gyres. These cells are driven by the attendant anomalous eddy momentum flux and help extend the wind anomalies from the upper troposphere to the near surface.

[39] The appearance and persistence of the surface NAM is inexorably tied to the mean circulation and the momentum forcing. The ring-like NAM pattern (of positive phase) becomes clearly evident after the growth stage. The growth of the surface NAM index toward larger positive values parallels the growth of poleward momentum flux and the persistence of the high positive NAM state coincides with

the momentum flux around the latter stage of the life cycle [*Ambaum and Hoskins*, 2002; *Norton*, 2003].

[40] Anomalous heat flux poleward of 50°N becomes significant throughout the atmosphere, coincident with pronounced momentum forcing. Between days −20 to +20, reduced poleward heat flux is observed as the vortex becomes strongest; increased poleward heat flux is observed as the vortex recovers. While this behavior is similar to SSW, around day 0, we note a strong and significant response in poleward heat flux below 300 hPa in connection with synoptic wave activity (of wave number 4 and greater) that was not obvious in the case of SSWs. This suggests anomalous wave activity poleward of 50°N by weather systems when the NAM becomes positive and the vortex is strongest. This is consistent with the baroclinic eddy feedback mechanism proposed by *Robinson* [2000].

[41] In our preliminary examination, the anomalous vortex intensification seems to occur preferentially during La Niña conditions. Assuming a 50% probability of a SSW occurrence in any given year, the resulting SSW events tend to coincide with El Niño years. However, the role of the tropical tropospheric forcing in vortex variability is still largely unexplored. Taguchi and Hartmann (submitted manuscript, 2005) demonstrated in their model experiments that SSWs are about twice as probable during El Niño as during La Niña. Furthermore, these authors find that the effect of prior SSWs interfere positively with ENSO signals over North America to produce enhanced interannual variations in wintertime climate [*Taguchi and Hartmann*, 2005]. Recent work by *Chen et al.* [2003] suggests that stratospheric planetary waves are strongly influenced by ENSO. They find that planetary waves tend to be refracted poleward (equatorward) during El Niño (La Niña) which is consistent with SSW tendency during El Niño years. Furthermore, they find that fluctuations in wave refraction are moderately correlated with the PNA pattern. Changes in tropospheric flow associated with the PNA pattern may alter the upward and meridional propagation of planetary waves as they penetrate the lower stratosphere [*Baldwin and O'Sullivan*, 1995]. Like the NAM, the PNA is a naturally occurring pattern of atmospheric variability, related to internal atmospheric dynamics, and reflects large-scale changes in tropospheric jet and weather patterns. For monthly analysis poleward of 20°N, PNA is indeed the second leading mode of variability of sea level pressure and surface air temperature behind the NAM [*Quadrelli and Wallace*, 2002, 2004].

[42] Overall, the VI results shown here illustrate that the behavior of anomalous atmospheric flows and wave activity is not the exact opposite that of SSWs. As such, lag correlation or similar linear analysis used to decipher the evolution of the polar vortex variability may not observe the behavior shown in the present study.

[43] **Acknowledgments.** The NCEP/NCAR Reanalysis data and Interpolate OLR data are provided by the NOAA-CIRES Climate Diagnostics Center, Boulder, Colorado, from their Web site at http://www.cdc.noaa.gov. The NINO3.4 index is provided by NOAA Climate Prediction Center, Camp Springs, Maryland, from their website at http://www.cpc.ncep.noaa.gov/data/indices/index.html. The authors thank the anonymous reviewers whose comments significantly improved the manuscript. V.L. is supported by the National Science Foundation (NSF) under grant ATM-0213248. D.L.H. is supported by the NSF under grant ATM-9873691 from the Climate Dynamics Program. D.W.J.T. is supported by NSF under grants CAREER: ATM-0132190 and ATM-0320959. Y.L.Y. was supported by NASA grants NAG1-1806 and NNG04N02G.

References

Andrews, D. G., J. R. Holton, and C. B. Leovy (1987), *Middle Atmospheric Dynamics*, 489 pp., Elsevier, New York.

Ambaum, M. H. P., and B. J. Hoskins (2002), The NAO troposphere-stratosphere connection, *J. Clim.*, *15*, 1969–1978.

Baldwin, M. P., and T. J. Dunkerton (1999), Propagation of the Arctic Oscillation from the stratosphere to the troposphere, *J. Geophys. Res.*, *104*, 30,937–30,946.

Baldwin, M. P., and T. J. Dunkerton (2001), Stratospheric harbingers of anomalous weather regimes, *Science*, *294*, 581–584.

Baldwin, M. P., and D. O'Sullivan (1995), Stratospheric effects of ENSO-related tropospheric circulation anomalies, *J. Clim.*, *8*, 649–667.

Black, R. X. (2002), Stratospheric forcing of surface climate in the Arctic Oscillation, *J. Clim.*, *15*, 268–277.

Chen, W., M. Takahashi, and H.-F. Graf (2003), Interannual variations of stationary planetary wave activity in the northern winter troposphere and stratosphere and their relationship to NAM and SST, *J. Geophys. Res.*, *108*(D24), 4797, doi:10.1029/2003JD003834.

Hartley, D. E., J. Villarin, R. X. Black, and C. A. Davis (1998), A new perspective on the dynamical link between the stratosphere and troposphere, *Nature*, *391*, 471–474.

Hartmann, D. L., J. M. Wallace, V. Limpasuvan, D. W. J. Thompson, and J. R. Holton (2000), Can ozone depletion and global warming interact to produce rapid climate change?, *Proc. Natl. Acad. Sci. U.S.A.*, *97*, 1412–1417.

Haynes, P. H., C. J. Marks, M. E. McIntyre, T. G. Shepherd, and K. P. Shine (1991), On the "downward control" of extratropical diabatic circulations by eddy-induced mean zonal forces, *J. Atmos. Sci.*, *48*, 651–679.

Holton, J. R., and H.-C. Tan (1980), The influence of the equatorial quasi-biennial oscillation on the global circulation at 50 mb, *J. Atmos. Sci.*, *37*, 2200–2208.

Kalnay, M. E., et al. (1996), The NCEP/NCAR reanalysis project, *Bull. Am. Meteorol. Soc.*, *77*, 437–471.

Kodera, K., M. Chiba, H. Koide, A. Kitoh, and Y. Nikaidou (1996), Interannual variability of the winter stratosphere and troposphere, *J. Meteorol. Soc. Jpn.*, *74*, 365–382.

Kuroda, K. (2002), Relationship between the Polar-Night Jet Oscillation and the Annular Mode, *Geophys. Res. Lett.*, *29*(8), 1240, doi:10.1029/2001GL013933.

Kuroda, Y., and K. Kodera (1999), Role of planetary waves in the stratosphere-troposphere coupled variability in the Northern Hemisphere winter, *Geophys. Res. Lett.*, *26*, 2375–2378.

Liebmann, B., and C. A. Smith (1996), Description of a complete (interpolated) outgoing longwave radiation dataset, *Bull. Am. Meteorol. Soc.*, *77*, 1275–1277.

Limpasuvan, V., and D. L. Hartmann (2000), Wave-maintained annular modes of climate variability, *J. Clim.*, *13*, 4414–4429.

Limpasuvan, V., D. W. J. Thompson, and D. L. Hartmann (2004), The life cycle of the Northern Hemisphere sudden stratospheric warmings, *J. Clim.*, *17*, 2584–2596.

Lorenz, D. J., and D. L. Hartmann (2003), Eddy-zonal flow feedback in the Northern Hemisphere winter, *J. Clim.*, *16*, 1212–1227.

McIntyre, M. E. (1982), How well do we understand the dynamics of stratospheric warming, *J. Meteorol. Soc. Jpn.*, *60*, 37–64.

Naito, Y., and I. Hirota (1997), Interannual variability of the northern winter stratospheric circulation related to the QBO and the solar cycle, *J. Meteorol. Soc. Jpn.*, *75*, 925–937.

North, G. R. T., et al. (1982), Sampling errors in the estimation of empirical orthogonal functions, *Mon. Weather Rev.*, *110*, 699–706.

Norton, W. A. (2003), Sensitivity of Northern Hemisphere surface climate to simulation of the stratospheric polar vortex, *Geophys. Res. Lett.*, *30*(12), 1627, doi:10.1029/2003GL016958.

O'Neill, A. (1980), The dynamics of stratospheric warmings generated by a general-circulation model of the troposphere and stratosphere, *Q. J. R. Meteorol. Soc.*, *106*, 659–690.

O'Neill, A., and B. F. Taylor (1979), Study of the major stratospheric warming of 1976–77, *Q. J. R. Meteorol. Soc.*, *105*, 75–92.

Plumb, R. A., and R. C. Bell (1982), A model of the quasi-biennial oscillation on an equatorial beta-plane, *Q. J. R. Meteorol. Soc.*, *108*, 335–352.

Polvani, L. M., and P. J. Kushner (2002), Tropospheric response to stratospheric perturbations in a relatively simple general circulation model, *Geophys. Res. Lett.*, *29*(7), 1114, doi:10.1029/2001GL014284.

Quadrelli, R., and J. M. Wallace (2002), Dependence of the structure of the Northern Hemisphere annular mode on the polarity of ENSO, *Geophys. Res. Lett.*, *29*(23), 2132, doi:10.1029/2002GL015807.

Quadrelli, R., and J. M. Wallace (2004), A simplified linear framework for interpreting patterns of Northern Hemisphere wintertime climate variability, *J. Clim.*, *17*(19), 3728–3744.

Quiroz, R. S. (1977), The tropospheric-stratospheric polar vortex breakdown of January 1977, *Geophys. Res. Lett.*, *4*, 151–154.

Robinson, W. A. (2000), A baroclinic mechanism for the eddy feedback on the zonal index, *J. Atmos. Sci.*, *57*(3), 415–422.

Ruzmaikin, A., J. Feynman, X. Jiang, and Y. L. Yung (2005), Extratropical signature of the Quasi-Biennial Oscillation, *J. Geophys. Res.*, *110*, D11111, doi:10.1029/2004JD005382.

Shindell, D. T., R. L. Miller, G. A. Schmidt, and L. Pandolfo (1999), Simulation of recent northern winter climate trends by green-house-gas forcing, *Nature*, *399*, 452–455.

Taguchi, M., and D. L. Hartmann (2005), Interference of extratropical surface climate anomalies induced by El Niño and stratospheric sudden warmings, *Geophys. Res. Lett.*, *32*, L04709, doi:10.1029/2004GL022004.

Thompson, D. W. J., and J. M. Wallace (1998), The Arctic Oscillation signature in the wintertime geopotential height and temperature fields, *Geophys. Res. Lett.*, *25*, 1297–1300.

D. L. Hartmann, Department of Atmospheric Sciences, University of Washington, Seattle, WA 98195, USA.

K. Jeev, Department of Earth and Planetary Sciences, Johns Hopkins University, Baltimore, MD 21218, USA.

V. Limpasuvan, Department of Chemistry and Physics, Coastal Carolina University, P.O. Box 261954, Conway, SC 29528, USA. (var@coastal.edu)

D. W. J. Thompson, Department of Atmospheric Science, Colorado State University, Fort Collins, CO 80523, USA.

Y. L. Yung, Division of Geological and Planetary Sciences, California Institute of Technology, Pasadena, CA 91125, USA.